Assessing the Impact of Diffuse Fraction Estimation on Ground Albedo Modeling

Juan M. Rodríguez-Muñoz, Rodrigo Alonso-Suárez, Italo Bove and Gonzalo Abal

Laboratorio de Energía Solar, Universidad de la República (Uruguay)

Abstract

Ground reflectivity or albedo is required for the estimation of the solar irradiance incident on an inclined surface. The ground is frequently modeled as a constant albedo diffuse reflector and this is inadequate for several solar energy applications, particularly for bifacial PV power plant yield estimation. Recent advances have categorized albedo models according to their complexity, with bivariate models -those incorporating the zenith angle and diffuse fraction- performing better. In a previous study, Rodríguez-Muñoz et al. (2022) evaluated six albedo models and confirmed that bivariate models were the most accurate. However, they also highlighted the need for measurements of both global and diffuse solar irradiance to apply these models. For simplicity, empirical diffuse fraction models can be used instead of using diffuse irradiance measurements. This study builds upon prior research by assessing the impact of employing empirical diffuse fraction models on albedo estimation. To assess this, measurements were conducted over the course of approximately one year at an experimental site with soil and climate conditions representative of the Pampa Húmeda region in South America. The results indicate that incorporating these models into albedo estimation slightly degrades performance, but still outperforms constant and univariate models. Thus, a bivariate albedo model combined with diffuse fraction estimates represents an effective balance between accuracy and simplicity.

Keywords: ground albedo, diffuse fraction, bifacial PV.

1. Introduction

Solar energy applications require estimating global solar irradiance on surfaces of arbitrary orientation, which includes three components: direct irradiance, diffuse irradiance from the sky, and irradiance reflected from nearby surfaces. Traditional transposition models typically focus only on ground reflection, assuming it to be hemispherical and isotropic reflecting surface with constant albedo. This assumption is generally sufficient when the reflected component constitutes a small portion of the total incident irradiance, as in many solar energy applications. However, this assumption is less suitable for bifacial photovoltaic panels, which are more sensitive to ground reflection. These panels can generate up to 15% more energy annually than conventional panels on typical albedo soils, and up to 30% more on highly reflective soils (Yusufoglu et al., 2014). The increasing adoption of this technology suggests it will soon dominate the market (Kopecek & Libal, 2021). This trend has motivated the advancement of more sophisticated albedo models that take into account solar geometry, cloud cover, and the characteristics of the surrounding terrain.

These models fall into three categories of increasing complexity. The first category (I) includes models that assume that the ground is a diffuse hemispherical isotropic reflector with a constant albedo. Variations in these models arise from different methods for assigning this constant value (Liu & Jordan, 1960; Gueymard, 1987; Psiloglou & Kambezidis, 2009). The second category (II) includes models that introduce some specular component in the reflected ground irradiance, thus treating albedo as a univariate function of the solar zenith angle (Nkemdirim, 1972; Temps & Coulson, 1977; Dickinson, 1983; Psiloglou & Kambezidis, 2009; Tuomiranta et al., 2021). The third category (III) includes models that further refines the previous by incorporating cloudiness information (through the diffuse fraction) into the albedo calculation (Temps & Coulson, 1977; Gueymard, 1987; Gardner & Nadeau, 1988; Ineichen et al., 1990; Chiodetti et al., 2016; Tuomiranta et al., 2021). These latter models require measurements of both global and diffuse horizontal irradiance, whereas the simpler models in the first two categories only need global irradiance.

Comparative performance of these models across different soils and climates has been explored in the literature (Ineichen et al., 1990; Psiloglou & Kambezidis, 2009; Tuomiranta et al., 2021). Early studies recommended using constant, locally measured albedo values based on terrain characteristics (Ineichen et al., 1990). However, more recent research, such as Tuomiranta et al. (2021), which evaluated 26 albedo models at 26 sites, reports significant

Selection and/or peer review under responsibility of Scientific Committee
10.18086/eurosun.2024.10.05 Available at http://proceedings.ises.org

benefits of using bivariate models. Their findings also suggest that relying on constant albedo values from databases can introduce significant errors, highlighting the need for local model adaptation to reflect typical conditions accurately.

Given the importance of local adaptation, Rodríguez-Muñoz et al. (2022) evaluated the performance of six pre-existing models for estimating green grass albedo using data from a site in the Pampa Húmeda region in South America (Salto, Northwest of Uruguay). Two models from each category were selected based on Tuomiranta et al. (2021). The best-performing model was identified both globally and within each category. The models' coefficients were determined through random sampling and cross-validation using albedo measurements from the Solar Energy Laboratory at the University of the Republic of Uruguay (LES-UdelaR). The most accurate models were those in the third category, which are bivariate and depend on the Sun position in the sky and the diffuse fraction. However, these models are more complex to implement and calibrate locally, as they require the additional measurement of horizontal diffuse irradiance (DHI) for the calculation of the diffuse fraction, $f_d = \mathrm{DHI}/\mathrm{GHI}$, where GHI is the horizontal global solar irradiance. Datasets with DHI are less common than those with GHI, since the accurate measurement of the diffuse component requires precise solar tracking for blocking the direct and circumsolar components and this implies frequent maintenance.

An alternative approach to simplify the implementation of bivariate albedo models is the use of empirical diffuse fraction models. These models estimate the diffuse fraction through empirical correlations based on geometrical calculations and global irradiance data, such as the solar zenith angle and clearness index, thus eliminating the need for measurements of diffuse solar irradiance (Abal et al., 2017; Yang, 2022). This study aims to assess the impact on model performance when using empirical diffuse fraction models instead of diffuse solar irradiance measurements.. Specifically, it considers two locally adjusted diffuse fraction models in combination with two bivariate locally adjusted albedo models. The performance of these combinations was assessed using one year of quality-controlled albedo measurements collected at LES-UdelaR, which were independent of the data used in the previous work (Rodríguez-Muñoz et al., 2022). The coefficients of the albedo models were updated due to minor differences in grass height at the site, compared to the previous campaign.

This paper is organized as follows: The next section provides an overview of the models under consideration (both for albedo and diffuse fraction), details the dataset used, outlines the quality control procedures, and describes the performance indicators for model comparison. This is followed by a presentation and analysis of the results. The final section summarizes the main conclusions of this study.

2. Methodology

2.1. Albedo models

The albedo or reflectance of a surface is the fraction of global solar irradiance that is reflected by it. The albedo of the ground, assumed horizontal, is defined as:

$$\rho_g = \frac{G_g}{G_h} \tag{1}$$

where G_g is the irradiance reflected by the ground (to the entire hemisphere) and G_h is the global solar irradiance on a horizontal plane. This parameter depends on various factors: solar altitude, cloudiness, changes due to local climate or human actions (e.g., changes in the surrounding terrain or grass height due to maintenance). The simplest model assumes the ground to be a diffuse hemispherical isotropic reflector with constant albedo independent of the aforementioned variables. The albedo can be obtained from generic databases for different soil types (Liu & Jordan, 1960; Gueymard, 1987) or estimated from experimental measurements, this latter being the recommended procedure (Ineichen et al., 1990; Tuomiranta et al., 2021).

Although this work focuses on bivariate models (category III), it will also include category I and II models to provide a better framework and baseline for comparison, working with a total of four albedo models. The first model considered in this work the arithmetic mean albedo,

$$model\ 1: \rho_g = \frac{1}{n}\sum \rho_i \tag{2}$$

where ρ_i represents the i-th albedo measurement out of n measurements. This model belongs to category I and is considered in Psiloglou & Kambezidis (2009) and Tuomiranta et al. (2021).

The second model in this work corresponds to that proposed by Tuomiranta et al. (2021)

$$model\ 2: \rho_g = \rho_n \times \frac{1 + b_1}{1 + b_1 cos\theta_z} \quad (3)$$

This univariate model depends on the solar zenith angle, θ_z, and has two adjustable parameters: ρ_n and b_1. Is based on the previous work of Dickinson (1983) and involves the restriction: $b_1 \in [0, 2]$, indicating that albedo is an increasing function of the solar zenith angle. This directional model is in category II.

Although there exist other models in categories I and II, the models selected for this study offer the highest performance within their categories for the specific ground and climate conditions considered here. This is supported by the findings of Tuomiranta et al. (2021) and Rodríguez-Muñoz et al. (2022).

The third and fourth models are bivariate and belong to category III. Specifically, the third model extends the second model and as proposed by Tuomiranta et al. (2021). It incorporates cloud cover presence through the diffuse fraction f_d and features three adjustable parameters. This approach allows for separate consideration of reflections from both direct and diffuse solar irradiance:

$$model\ 3: \rho_g = (1 - f_d) \times \rho_{bn} \times \frac{1 + b_1}{1 + b_1 cos\theta_z} + f_d \times \rho_d \quad (4)$$

where ρ_{bn}, b_1, and ρ_d are the adjustable parameters. The parameters ρ_{bn} and ρ_d represent the albedo for beam solar irradiance and diffuse solar irradiance, respectively. The restriction $b_1 \in [0, 2]$ is maintained, and the condition $\rho_{bn} \leq \rho_d$ is added.

The fourth and final model has a similar structure, and was initially proposed by Rodríguez et al. (2022). It builds on Gueymard's (1987) model for inclined surfaces, but has been adapted and simplified for horizontal surfaces. It integrates both the zenith angle and the diffuse fraction into a simplified expression with five adjustable parameters:

$$model\ 4: \rho_g = (1 - f_d) \times \left[\rho_n + e^{b_1 + b_2\theta_z + b_3\theta_z^2}\right] + f_d \times \rho_d \quad (5)$$

where ρ_n represents the albedo for direct normal irradiance under pure isotropy conditions, and ρ_d is the albedo for diffuse irradiance. The parameters b_1, b_2, and b_3 control how the albedo varies with the solar zenith angle. This model has five adjustable parameters in total.

2.2. Diffuse fraction models

As mentioned in the introduction, category III models require two experimental measurements: GHI and DHI. This work explores the cost -in terms of accuracy- of replacing the DHI measurements with a locally adjusted phenomenological model to estimate DHI from GHI.

Numerous phenomenological models for diffuse fraction estimation are used worldwide (see Yang (2022) for a comprehensive review). However, these models often require locally adapted coefficients to perform with acceptable accuracy in different climates. For convenience and simplicity, we selected two of the simplest and best performing models from Abal et al. (2017), which also used data from a site in Salto.

The first model, referred here as RA2s (Ruiz Arias et al., 2010), has a dependence on air mass (or solar zenith angle) and on the clearness index (or GHI), as shown in Eq. (6). The second model, referred here as SO2, is the historical model introduced in Skartveit and Olseth (1987). It has a more complicated structure than RA2s but ultimatley depends on the solar altitude (or solar zenith angle) and the clearness index. Both models, were previously evaluated with locally adjusted coefficients for the Salto site, have a relative RMSD of 16.9% and 16.6% of the measured diffuse fraction, respectively and negligible mean bias (Abal et al. (2017)). As mentioned, both are bivariate and require the clearness index ($k_t = GHI/S_C\ F_n cos(\theta_z)$, a normalized version of the GHI defined below) and the solar zenith angle, which can be calculated from site position and local time information.

The RA2s model is given by the following expression:

$$RA2s\ model: f_d = a_0 + a_1 \times e^{-exp(a_2 + a_3 k_t + a_4 k_t^2 + a_5 m)} \quad (6)$$

where k_t is the clearness index defined as $k_t = G_h/G_{0h}$, where $G_{0h} = S_c F_n cos(\theta_z)$ is the solar irradiance on a horizontal surface at the top of the atmosphere (with a solar constant Sc = 1361 W/m^2 and F_n the orbital factor). The parameter *m* represents the air mass and is calculated from the zenith angle including corrections for sphericity and refraction (Young 1994). The RA2s model has six adjustable parameters: a_0, a_1, a_2, a_3, a_4, a_5.

The SO2 model is shown below,

$$SO2\ model: f_d = \begin{cases} 1 & k_t < k_a \\ f(k_t, \alpha_s) & k_a \le k_t \le \alpha k_b(\alpha_s) \\ f(\alpha k_t, \alpha_s) & k_t > \alpha k_b(\alpha_s) \end{cases} \quad (7)$$

with,

$$\begin{aligned} f(k_t, \alpha_s) &= 1 - (1 - d_1)\left[a\sqrt{K} + (1 - a)K^2\right], \\ K(k_t, \alpha_s) &= \frac{1}{2}\left\{1 + sin\left[\pi\left(\frac{k_t - k_a}{k_b - k_a} - \frac{1}{2}\right)\right]\right\}, \\ k_b(\alpha_s) &= r + sexp\left(\frac{-\alpha_s}{\alpha_0}\right), \\ d_1(\alpha_s) &= r' + s'exp\left(\frac{-\alpha_s}{\alpha_0}\right), \end{aligned} \quad (8)$$

where α_s is the solar altitude and the complementary angle of the zenith angle, and α_0=0.291. This model also has six adjustable parameters: a, k_a, r, s, r′, and s′.

The locally determined parameters for both models, specific to the location of this work (Salto), can be found in Abal et al. (2017).

2.3 Experimental data and quality control

The experimental data for this study was collected at the Solar Energy Laboratory of the University of the Republic of Uruguay (LES-UdelaR, from its Spanish name), located in a semi-rural area near the city of Salto (latitude: 31.28°S, longitude: 57.92°W, altitude: 60 m above sea level). LES is located in the Pampa Húmeda climate region, classified as Cfa (warm temperate, humid, with hot summers) according to the updated Köppen-Geiger classification (Peel et al., 2007). The data results from a setup deviced specifically to measure ground albedo and set spans approximately one year, from January 2023 to January 2024. It includes global horizontal irradiance (G_h or GHI), solar irradiance reflected by the ground with no tilt (G_g), diffuse horizontal irradiance (G_d or DHI), and normal incidence solar irradiance (G_b or DNI) recorded at one-minute intervals.

Fig. 1a: Albedo measurement setup, including G_h and G_g sensors (both instruments on the right; the others are for inclined solar irradiance, not used in this study).

Fig. 1b: SOLYS2 system with G_d and G_b sensors.

Fig. 1: Installation of measuring instruments.

The ground under study is covered mainly by green grass, and its albedo was calculated using Eq. (1) with measurements of G_g and G_h. These measurements were taken with Kipp & Zonen CMP6 pyranometers positioned 1.2 meters above the ground, using a special support shown in Fig. 1a (both equipment at the right). Horizontal diffuse solar irradiance, G_d, was measured with a Kipp & Zonen CMP10 ventilated pyranometer with a shading ball,

mounted on a SOLYS2 tracking system (Fig. 1b), located about 30 meters from the previous setup. Direct normal irradiance was measured with a Kipp & Zonen CHP1 pyrheliometer on the same tracking system, primarily for quality control. All pyranometers are maintained daily and calibrated twice a year against the LES secondary standard, which is traceable to the World Standard Group in the World Radiation Center in Davos, Switzerland. Data were recorded every minute and averaged over ten-minute intervals to account for spatial mismatch between measurements and to account for rapid irradiance variations due to specific cloud formations.

The diurnal dataset (N=22282 records) was subjected to a series of quality control filters based on the Baseline Solar Radiation Network guidelines (BSRN; McArthur (2005)). The quality control process is summarized in Table 1 and Fig. 2. Each filter is applied on diurnal records, independently from the rest, except for the last one. The first four filters (F1 to F4) apply upper and lower limits to the solar irradiance measurements, G, as follows:

$$b \leq G \leq S_c p(cos\theta_z)^a + c \quad (9)$$

where G represents each solar irradiance component and parameters *p*, *a*, *b*, and c were determined locally for each filter through visual inspection. Filter F5 imposes a lower limit on solar altitude, $\alpha_s > 10°$, excluding measurements affected by significant directional errors (low solar altitudes). Filter F6 checks that G_h, G_d, and G_b satisfy the closure relation:

$$G_h = G_b cos\theta_z + G_d \quad (10)$$

with an 8 % tolerance from the average G_h. Filter F7 imposes an upper limit on the diffuse fraction, ensuring that f_d <1.03, with a 3 % tolerance to allow for experimental error. Filter F8 eliminates data points with low clearness index and low diffuse fraction, typically linked to errors under heavy overcast conditions and low irradiance. Filter F9 sets a loose upper limit on the clearness index, with $k_t < 1$. Filter F10 ensures albedo measurements are within the theoretical range $0 \leq \rho_g \leq 1$. Finally, Filter F11 is a statistical filter that removes outliers, defined as albedo data not meeting the condition $\left|\rho_g - \overline{\rho}_g\right| \leq 3\sigma$, where $\overline{\rho}_g$ and σ represent the mean and standard deviation of albedo measurements in the corresponding interval. This filter is applied independently in data bins defined by 10-degree zenith angle intervals, following the application of filters F1 to F11. At the end of this process, approximately 43 % of the original data was discarded, with 14 % removed due to solar altitude (F5). Table 1 provides details on each filter's conditions, the variables affected, the number of passing data points, and those discarded.

Tab. 1: Detail of the filtering process applied to the diurnal measurements

Filter	condition	variable	output	% discarded
F1	Eq. (9)	G_h	20749	6.9
F2	Eq. (9)	G_d	18304	17.9
F3	Eq. (9)	G_b	21724	2.5
F4	Eq. (9)	G_d	19930	10.6
F5	$\alpha_s > 10°$	all	19102	14.3
F6	Eq. (10)	G_h, G_d, G_b	18549	16.8
F7	$f_d < 1.03$	G_h, G_d	16860	24.3
F8	$k_t < 0.20$ & $f_d > 0.80$	G_h, G_d	21313	4.4
F9	$k_t < 1$	G_h	22269	0.0
F10	$0 \leq \rho_g \leq 1$	G_g, G_h	19866	10.8
F11	$\left\|\rho_g - \overline{\rho}_g\right\| \leq 3\sigma$	G_g, G_h	15949	28.4
all	-	all	12698	43.0

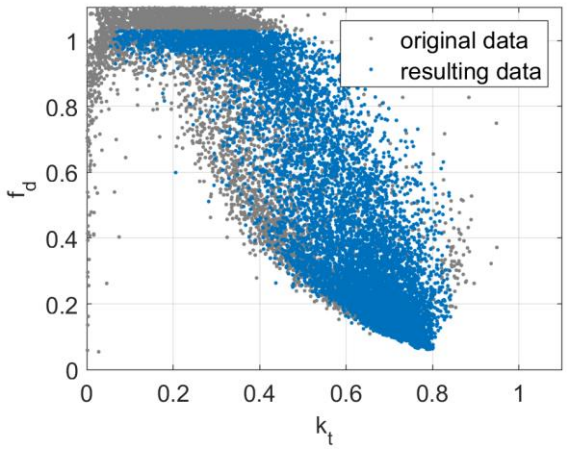

Fig. 2a: Diffuse fraction vs clearness index.

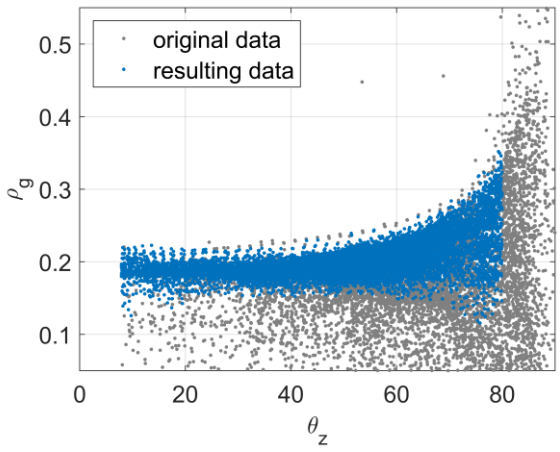

Fig. 2b: Albedo vs zenith angle.

Fig. 2: Result of the filtering procedure: original data in gray and data resulting from the filtering procedure in blue (those that pass all filters).

2.3 Methodology and performance indicators

The methodology employed in this work has three parts. First, the filtered dataset was employed to update the coefficients of the previously described albedo models. For Model 1, the arithmetic mean of the albedo measurements was calculated using Eq. (2). For Models 2 to 4, regression algorithms were utilized to minimize the mean squared error between measured and modeled albedo. For this part, the measured diffuse fraction was used for Models 3 and 4, without imposing any optimization parameter constraints. In the second part of the study, the performance of the diffuse fraction models RA2a and SO2 was evaluated. Finally, in the third part, the performance of Models 3 and 4 was reassessed using diffuse fraction estimates derived from the RA2a and SO2 models.

The coefficients from previous work (Rodríguez-Muñoz et al, 2022) were not utilized due to differences in the experimental setup and grass height, which may influence the albedo. Efforts were made to maintain a relatively constant grass height in a broad circle around the setup throughout the year, but the data may contain seasonal trends, since different amounts of rainfall and air temperature between summer and winter may seasonally affect the albedo of the grass. To update model coefficients and performance indicators, random sampling and cross-validation were employed, with 60% of the data utilized for training and 40% for validation. To ensure the consistency of the results, the 60/40 split was repeated 1,000 times, and the final results are the average of the coefficients and the performance indicators, respectively.

The model performance was evaluated using three indicators: mean bias deviation (MBD), root mean squared deviation (RMSD), and Kolmogorov-Smirnov integral (KSI). These are defined as follows:

$$MBD = \frac{1}{n}\sum_{i=1}^{n}(\hat{y}_i - y_i), \qquad RMSD = \left[\frac{1}{n}\sum_{i=1}^{n}(\hat{y}_i - y_i)^2\right]^{1/2}, \qquad KSI = \int_0^1 \left|\hat{F}(y) - F(y)\right| dy, \tag{11}$$

where y_i represents the reference value (albedo measurement), $\hat{y}_i$ is the model estimate, and $F(y)$ and $\hat{F}(y)$ are the cumulative probability distributions of y_i and $\hat{y}_i$, respectively. These metrics share the same units as y_i, making them dimensionless for albedo measurements. They can also be expressed relatively (rMBD, rRMSD, and rKSI) as a percentage of the mean measurement value. Each indicator provides unique information about the model's accuracy: MBD shows the average bias of the estimates, RMSD gauges the spread of the estimation errors, and KSI quantifies the statistical distance between the cumulative distributions of measurements and estimates. In order to provide a unified representation of these indicators, the Combined Performance Indicator (CPI) has been defined, integrating the three metrics into a single one:

$$CPI = \frac{1}{3}(|rMBD| + rRMSD + rKSI) \tag{12}$$

A similar global indicator has been proposed in Gueymard (2014) and has been successfully used in evaluating diffuse fraction models (Abal et al., 2017) and correction factors for diffuse irradiance measurements (Rodríguez-Muñoz et al., 2021).

3. Results

3.1 Locally adjusted albedo models performance

Table 2 shows the locally adjusted coefficients for the albedo models. As mentioned before, the values presented in this table correspond to the average of the 1000 iterations of the sampling and cross-validation procedure.

Tab. 2: Coefficients for locally adjusted models.

Model	coefficients				
	ρ_n/ρ_{nb}	b_1	b_2	b_3	ρ_d
1 - Arithmetic average, Eq. (2)	0.2021	-	-	-	-
2 - Tuomiranta et al. (2021), Eq. (3)	0.1651	0.0039	-	-	-
3 - Tuomiranta et al. (2021), Eq. (4)	0.1692	0.9406	-	-	0.1862
4 - Modified Gueymard (1987), Eq. (5)	0.1618	-3.5233	-0.0209	0.0005	0.1859

The standard deviations of the coefficients were also calculated, which turned out to be at least 30 times smaller than the averages, the small variability indicates the robustness of the models and the adjustment methods. The parameters of the models from Tuomiranta et al. (2021) models satisfy the constraints $b_1 \in [0, 2]$ and $\rho_{bn} \leq \rho_d$, indicating that these constraints do not need to be imposed during the parameter adjustment procedure, at least for the data used in this particular study. The values of the coefficients ρ_n, ρ_{nb}, and ρ_d are slightly lower than those previously adjusted by Rodríguez-Muñoz et al. (2022). For instance, in the case of model 1, the average value decreased from 0.2209 to 0.2021. This discrepancy is likely due to differences in soil humidity or grass height, as investigated by Dickinson (1983), which found that albedo values are inversely proportional to grass height. The coefficients describing the variation of albedo with the zenith angle, b_1, b_2, and b_3, remain practically unchanged from those reported in Rodríguez-Muñoz et al. (2022).

The performance indicators for the four models are shown in Table 3 as a percentage of the mean albedo value, $\overline{\rho}_g = 0.2021$. The indicators and overall ranking are similar to those presented in Rodríguez-Muñoz et al. (2022). All models show a mean bias close to zero (<1%). Based on rRMSD, the models are ranked from worst to best from 1 to 4. Based on rKSI, they are ranked 1, 2, 4, and 3, while based on the combined indicator CPI, they are ranked 1, 2, 4, and 3. In general, model performance improves with complexity: bivariate models (3 and 4) perform best, followed by univariate models (2), and the constant model (1) performs worst. Category III models (bivariate) perform similarly. Model 3 performs slightly best according to CPI, followed closely by model 4. Although Model 4 has the lowest rRMSD, this does not compensate for the difference in rKSI (statistical similarity of distributions). The difference in performance is small enough to consider them with similar accuracy.

Tab. 3: Performance indicators for the four albedo models, expressed as a percentage of the mean measurement value, $\overline{\rho}_g = 0.2021$.

Model	Relative performance indicators (%)			
	rMBD	rRMSE	rKSI	CPI
1 - Arithmetic average, Eq. (2)	0.0	12.2	8.9	7.0
2 - Tuomiranta et al. (2021), Eq. (3)	-0.7	9.4	2.6	4.0
3 - Tuomiranta et al. (2021), Eq. (4)	0.0	8.3	1.7	3.3
4 - Modified Gueymard (1987), Eq. (5)	0.0	7.9	2.6	3.5

Complementing the previous analyses, Fig. 3 shows the comparison of albedo measurements with model estimates in ρ_g vs. θ_z plots. Model 2 (Fig. 3a) generally describes the increasing behavior of albedo with solar zenith angle but does not capture the data scatter due to variations in cloud conditions. Model 3 (Fig. 3b) on the other hand, captures both the zenith angle dependence and the cloud condition dependence. Model 4 shows a similar behavior o its plot is omitted.

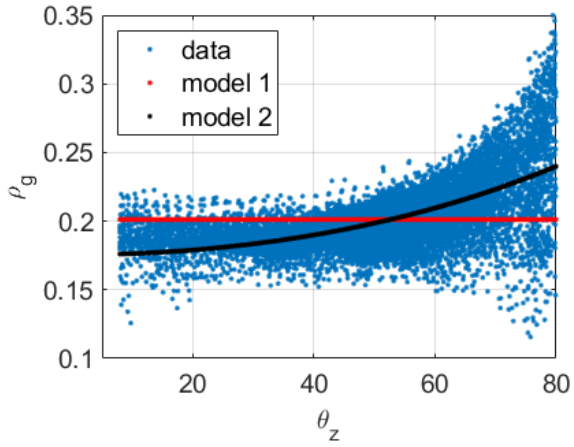

Fig. 3a: Model 1 and 2.

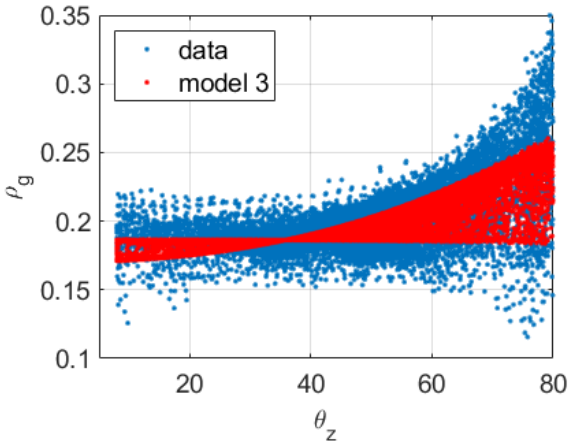

Fig. 3b: Model 3.

Fig. 3: Comparison between albedo measurements and estimates from different models.

3.2 Diffuse fraction model performance

As mentioned in the introduction, there is a plethora of phenomenological models for estimating the diffuse fraction from clearness index, solar zenith angle and other variables. A comprehensive review considering the performance of 140 published models against quality 1-minute data from 54 sites worldwide was published in 2016 (Gueymard and Ruiz-Arias, 2016). This work assessed the models with their original coefficients, which were derived from diverse datasets under different climatic conditions. Furthermore, several coefficients were derived from hourly datasets and used for 1-minute estimation of diffuse fraction. A more recent review (Yang 2022) considered 10 of the best diffuse fraction models against a 1-min dataset with five years of 1-min data from several sites worldwide. In this case, the coefficients where adjusted by grouping the data by broad climate zones, making for 5 or 6 sets of coefficients covering the whole globe. If anything, this search for a "quasi-universal" diffuse fraction model strongly suggests to us that there is no such thing. For a good performance, a diffuse fraction model must be adjusted to local data.

Tab. 4: Performance indicators for the for the two diffuse fraction models, expressed as a percentage of the mean measurement value, $\overline{f}_d = 0.3710$.

Model	Relative performance indicators (%)			
	rMBD	rRMSD	rKSI	CPI
RA2s	-7.7	33.4	10.1	17.1
S02	-11.5	33.5	12.3	19.1

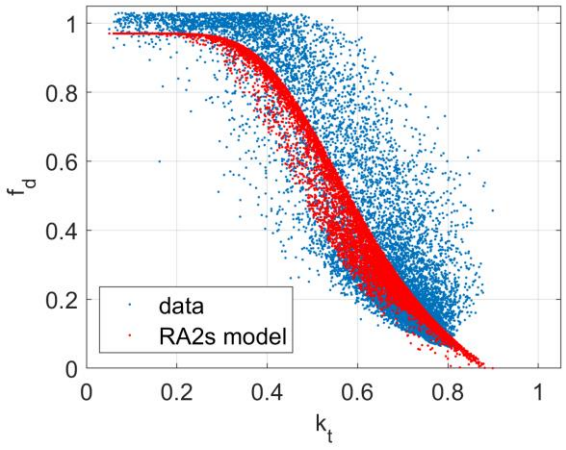

Fig. 4a: RA2s model.

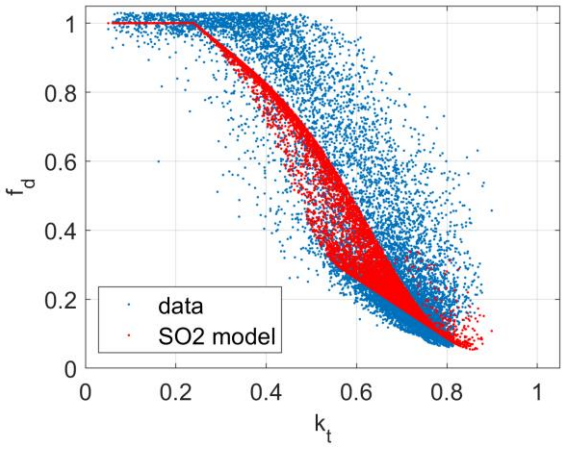

Fig. 4b: S02 model.

Fig. 4: Comparison between diffuse fraction measurements and estimates from different models.

Both models for diffuse fraction chosen for this work (RA2s Eq. (6) and SO2 Eq. (7)) are selected for its relative simplicity (they ultimately depend on the clearness index and the solar zenith angle) and because local adjusted sets for their coefficients are available for the site of interest in this work (Abal et al., 2017). These models estimate 10-minute diffuse fraction with rRMSD of about 33% and some underestimation is apparent in Fig. 4 and in the negative mean bias reported in Table 4. This may be due to the fact that coefficients adjusted to horuly data are being used on 10-min data. However, in the context of this paper, the interest is to evaluate the impact on accuracy of the albedo estimates of using even diffuse fraction models. To this objective, using poor diffuse fraction models is useful, as it may provide an upper value for the cost in terms of accuracy of the albedo estimates.

3.3 Impact of diffuse fraction estimation on bivariate albedo models

In this section, the impact of using phenomenological diffuse fraction models in combination with bivariate albedo models is evaluated. In this regard, Table 5 shows the performance indicators for the bivariate models considering three different scenarios, which differ in the way f_d is treated. In the first scenario, the experimental measurement of the diffuse fraction is used as a baseline (as in Table 3). In the second and third scenarios, f_d is estimated using the RA2s and SO2 models, respectively. The results show that the use of the phenomenological diffuse fraction models leads to a slight decrease in the performance metrics, with the smallest impact on rRMSD, followed by rMBD and rKSI. The models for the baseline scenario are unbiased, and they acquire small biases when diffuse fraction models are used. A negative bias in the fd estimation models translates to negative bias in albedo model 4 (subestimation of albedo) and to a positive bias in model 3 (overestimation of albedo). However, in both cases the mean biases are small, under 1%. Interestingly, the rRMSD (i.e., dispersion) of these models is almost unaffected by the use of diffuse fraction models. The performance of models 3 and 4 with f_d estimation still exceeds that of categories I and II, demonstrating the feasibility of combining empirical diffuse fraction models with category III ground albedo models when diffuse irradiance measurements are not available.

Tab. 5: Performance indicators for the four albedo models across three different scenarios, expressed as a percentage of the mean measurement value, $\overline{\rho}_g = 0.2021$.

Model	Approach for f_d	Relative performance indicators (%)			
		rMBD	rRMSD	rKSI	CPI
3 - Tuomiranta et al. (2021), Eq. (4)	Experimental (baseline)	0.0	8.3	1.7	3.3
	RA2s	0.3	8.3	1.9	3.5
	SO2	0.5	8.3	2.0	3.6
4 - Modified Gueymard (1987), Eq. (5)	Experimental (baseline).	0.0	7.9	2.6	3.5
	RA2s	-0.7	8.0	2.9	3.9
	SO2	-0.5	7.9	2.7	3.7

Complementing the previous analysis, Fig. 5 shows the rMBD and rRMSD for the best model 3 in scenarios 1 and 2, categorized by the cosine of the zenith angle ($\cos\theta_z$, *x* axis) and the clearness index (k_t, *y* axis). The clearness index correlates with the diffuse fraction and allows to distinguish between different sky conditions. Three different conditions can be identified: clear sky ($k_t > 0.6$), partly cloudy sky ($0.6 > k_t > 0.2$), and overcast sky ($k_t < 0.2$). These plots show under which sky conditions the performance of the model decreases. The results for the other cases are similar. The graphs use the same color scale to facilitate comparison, although in some cases the scale is saturated to ensure adequate visualization.

In Rodríguez-Muñoz et al. (2022), besides the general superiority of the category III models over the category I and II models, it was shown that they also exhibit a more homogeneous behavior when discriminating between sky conditions (diffuse fraction and solar elevation), i.e., the rRMSD and rMBE matrices are more uniform. This characteristic is maintained when diffuse fraction models are introduced, as can be seen in Fig. 5c and Fig. 5d. In these figures, it can be observed that the matrices do not change significantly in the range of the cosine of the zenith angle greater than 0.3, i.e. zenith angles less than about 70°, where the solar irradiance is higher. For zenith angles greater than 70°, more significant differences are observed, especially under clear sky conditions (kt > 0.6). It is also important to note that in these conditions the solar irradiance is lower, since these data correspond to the moment close to sunrise and sunset. Therefore, if the metrics were weighted by solar irradiance, the impact of diffuse fraction

models would be even smaller.

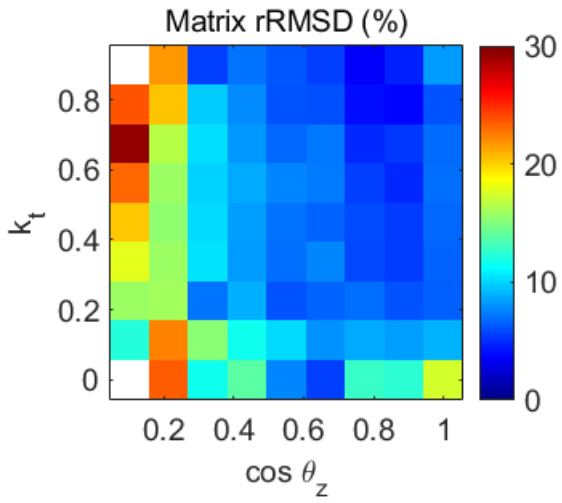

Fig. 5a: Model 3.

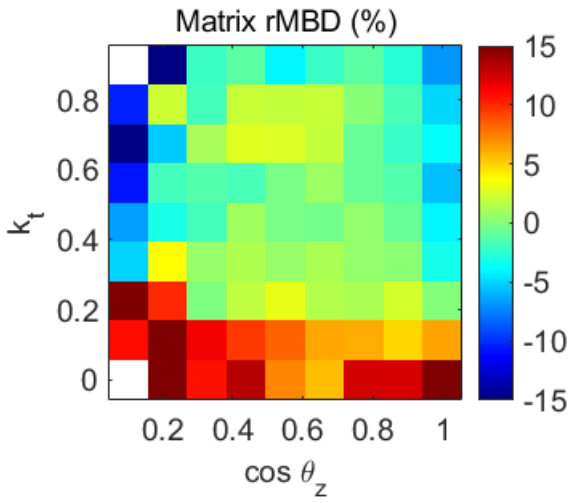

Fig. 5b: Model 3.

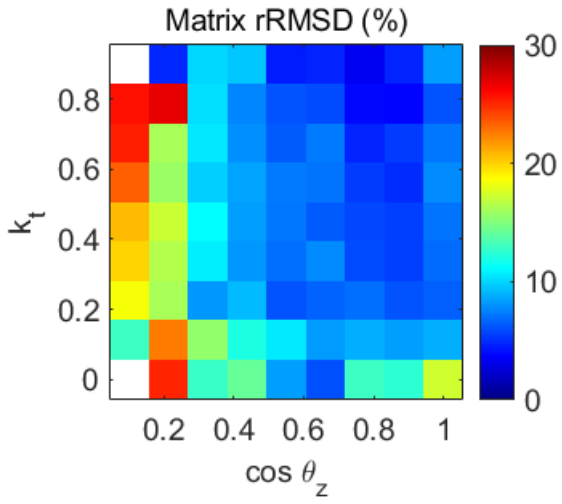

Fig. 5c: Model 3 combined with RA2s.

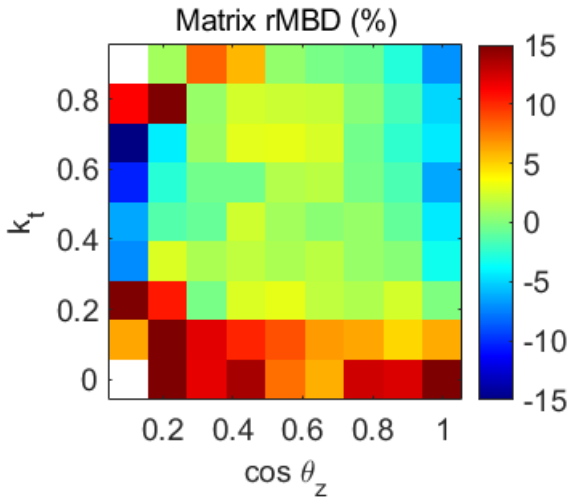

Fig. 5d: Model 3 combined with RA2s.

Fig. 5: rMBD and rRMSD matrix for the first and second scenario for model 3, expressed as a percentage of the mean measurement value, $\overline{\rho}_g = 0.2021$. The scale of the figures is the same to facilitate comparison. The white regions indicate that no data is available for that condition.

In the previous analysis, the coefficients adjusted for the specific site were used for the diffuse fraction models. The use of the original coefficients was also evaluated, but these results are not shown in this article because they are very similar. This reinforces the earlier conclusion: using empirical diffuse fraction models in conjunction with bivariate albedo models represents a robust option when diffuse solar irradiance measurements are not available.

4. Conclusions

The coefficients of four empirical albedo models for grass representative of the Pampa Húmeda region of South America were updated. The model coefficients were slightly lower than in the previous work (Rodríguez-Muñoz et al. 2022), probably due to differences in grass height between the measurement campaigns. Similarly, the performance indicators were very similar, and the conclusions regarding model performance are consistent with previous studies. The bivariate models show the best performance, followed by the univariate models and finally the constant models.

While the bivariate models perform better, their implementation is more challenging as they require two solar irradiance measurements: global and diffuse on a horizontal plane. In this context, with the aim of simplifying the implementation of these models, the impact of using empirical diffuse fraction models as a substitute for diffuse solar

irradiance measurements was evaluated, eliminating the need for one measurement. Despite the slight decrease in performance when diffuse fraction models are included, their superiority over categories I and II is evident. This supports the viability of combining empirical diffuse fraction models with category III albedo models, potentially creating a fourth category with performance between categories II and III while maintaining simplicity of implementation. These conclusions are considered valid regardless of whether the original coefficients or the locally adjusted coefficients are used for the diffuse fraction models, providing robustness to the models in this fourth category.

5. Acknowledgments

The authors thank the Sectoral Commission for Scientific Research (CSIC) of the University of the Republic for financial support through its R&D Groups program.

6. References

Abal, G., Aicardi, D., Alonso-Suárez, R., y Laguarda, A. (2017). Performance of empirical models for diffuse fraction in Uruguay. Solar Energy, 141:166–181.

Chiodetti, M., Lindsay, A., Dupeyrat, P., Binesti, D., Lutun, E., Radouane, K., y Mousel, S. (2016). PV bifacial yield simulation with a variable albedo model. En Proceedings of the EU PVSEC 2021.

Dickinson, R. E. (1983). Land surface processes and climate—surface albedos and energy balance. En Saltzman, B., editor, Theory of Climate, volumen 25 de Advances in Geophysics, pp. 305–353. Elsevier.

Gardner, C. L., y Nadeau, C. (1988). Estimating south slope irradiance in the arctic—a comparison of experimental and modeled values. Solar Energy, 41(3):227–240.

Gueymard, C. (1987). An anisotropic solar irradiance model for tilted surfaces and its comparison with selected engineering algorithms. Solar Energy, 38(5):367–386.

Gueymard, C. (2014). A review of validation methodologies and statistical performance indicators for modeled solar radiation data: Towards a better bankability of solar projects. Renewable and Sustainable Energy Reviews, 39:1024–1034.

Gueymard, C.A. and Ruiz-Arias, J.A. (2016), Extensive worldwide validation and climate sensitivity analysis of direct irradiance predictions from 1-min global irradiance, Solar Energy 128: pp 1-30.

Ineichen, P., Guisan, O., y Perez, R. (1990). Ground-reflected radiation and albedo. Solar Energy, 44(4):207–214.

Kopecek, R., y Libal, J. (2021). Bifacial photovoltaics 2021: Status, opportunities and challenges. Energies, 14(8).

Liu, B. Y., y Jordan, R. C. (1960). The interrelationship and characteristic distribution of direct, diffuse and total solar radiation. Solar Energy, 4(3):1–19.

McArthur, L. (2005). Baseline Surface Radiation Network (BSRN) Operations Manual. Td-no. 1274, wrcp/wmo, World Meteorological Organization (WMO). www.wmo.org.

Nkemdirim, L. C. (1972). A note on the albedo of surfaces. Journal of Applied Meteorology (1962-1982), 11(5):867–874.

Peel, M. C., Finlayson, B. L., y Mcmahon, T. A. (2007). Updated world map of the Köppen-Geiger climate classification. Hydrology and Earth System Sciences Discussions, 11:1633–1644. https://doi.org/10.5194/hess-11-1633-2007

Psiloglou, B., y Kambezidis, H. (2009). Estimation of the ground albedo for the Athens area, Greece. Journal of Atmospheric and Solar-Terrestrial Physics, 71(8):943–954.

Rodríguez-Muñoz, J. M., Monetta, A., Alonso-Suárez, R., Bove, I., y Abal, G. (2021). Correction methods for shadow-band diffuse irradiance measurements: assessing the impact of local adaptation. Renewable Energy, 178:830–844.

Rodríguez Muñoz, J. M., Alonso-Suárez, R., Bove, I., y Abal, G. (2022). Evaluación de seis modelos empíricos para estimar albedo del suelo en la Pampa Húmeda. En: Avances en Energías Renovables y Medio Ambiente, vol. 26, p. 357-368.

Ruiz-Arias, J. A., Alsamamra, H., Tovar-Pescador, J., y Pozo-Vázquez, D. (2010). Proposal of a regressive model for the hourly diffuse solar radiation under all sky conditions. Energy Conversion and Management, 51(5):881–893.

Skartveit, A., y Olseth, J. A. (1987). A model for the diffuse fraction of hourly global radiation. Solar Energy, 38(4):271–274.

Temps, R. C., y Coulson, K. (1977). Solar radiation incident upon slopes of different orientations. Solar Energy, 19(2):179–184.

Tuomiranta, A., Alet, P.-J., Ballif, C., y Ghedira, H. (2021). Worldwide performance evaluation of ground surface reflectance models. Solar Energy, 224:1063–1078.

Yang, D. (2022). Estimating 1-min beam and diffuse irradiance from the global irradiance: A review and an extensive worldwide comparison of latest separation models at 126 stations. Renewable and Sustainable Energy Reviews, 159:112195.

Young, A., 1994, "Air mass and refraction," Applied Optics, 33(6), pp. 1108-1110.

Yusufoglu, U. A., Lee, T. H., Pletzer, T. M., Halm, A., Koduvelikulathu, L. J., Comparotto, C., Kopecek, R., y Kurz, H. (2014). Simulation of energy production by bifacial modules with revision of ground reflection. Energy Procedia, 55:389–395. Proceedings of the 4th International Conference on Crystalline Silicon Photovoltaics (SiliconPV 2014).